Macromolecular Research, Vol. 13, No. 6, pp 499-505 (2005)

Synthesis and Characterization of Co-Surfactant Templated Mesoporous Materials with Enhanced Hydrothermal Stability

Geon-Joong Kim*

Department of Chemical Engineering, Inha University, Incheon 402-751, Korea

Hyun-Seok Kim, Yoon Soo Ko, and Yong Ku Kwon*

Department of Polymer Science and Engineering, Inha University, Incheon 402-751, Korea

Received July 21, 2005; Revised November 28, 2005

Abstract: Ordered mesoporous materials with a hydrothermally-stable, protozeolitic framework were prepared by exploring the direct conversion of inorganic species based on co-surfactant templating systems. To confer hydrothermal stability on the mesoporous materials, the organic-inorganic hybrids were heat-treated in strongly basic media. Co-surfactant templating systems of cetyltrimethylammonium bromide [$C_{16}H_{13}(CH_3)_3NBr$, CTAB] with 1,3,5-trimethylbenzene (TMB) or a nonionic block copolymer of poly(ethylene oxide)-*b*-poly(propylene oxide)-*b*-poly(ethylene oxide) ($EO_{20}PO_{70}EO_{20}$) were employed to improve the hydrothermal stability of the organic-inorganic self-assembly during the solid rearrangement process of the inorganic species. The mesoscopic ordering of the pore structure and geometry was identified by X-ray diffraction, small angle neutron scattering and electron microscopy.

Keywords: mesoporous materials, hydrothermal stability, mesoscopic ordering.

Introduction

Microporous materials with a pore diameter less than 1.5 nm have attracted a great deal of attention due to their interesting material characteristics, such as their large internal surface area, unique pore structure and adsorption capacity and controllability. A typical example is a crystalline zeolite material which exhibits thermal and hydrothermal stability and chemical resistance in a variety of catalytic uses.[1-4] Since the small pore size of these microporous materials is not adapted to the processing of large molecules on the nanometer level, however, recent research has been focused on the synthesis of nanoporous materials with a large pore size and uniform pore distribution.[5-9] Nanoporous materials with a pore diameter in the range of 1.5-10 nm would be suitable for a wide range of applications, e.g. selective catalysts for large molecules and cooperative complexes for enantioselective catalytic reactions.[10-12] Most of the procedures developed for the synthesis of these materials thus far use low molecular weight surfactants as a structure-directing agent and auxiliary inorganic precursors for assembly into the mesophase precipitant.[5-9] Amphiphilic block copolymers, which are structurally analogous to low molecular weight nonionic surfactants, can be used as a structure-directing agent to produce nanostructures with a larger pore size.[13-18]

Nanoporous molecular sieve materials exhibit relatively poor hydrothermal stability and are readily destroyed when exposed to steam or boiling water.[1-4] Furthermore, they exhibit weak acidity compared to microporous zeolite materials.[1-4] Therefore, a great deal of recent research has been devoted to enhancing the hydrothermal stability and acidity of this class of materials.[19-25] One particularly significant advance was made through the incorporation of zeolitic materials into the framework of the nanoporous materials.[26,27] Pinnavaia *et al.* used protozeolitic aluminosilicate nanoclusters or the so called zeolite seed materials as a framework precursor to form acidic and steam-stable aluminosilicate mesostructures.[21,22] Karlsson *et al.* demonstrated the direct conversion of inorganic species into a zeolite ZSM-5 crystal structure within the mesostructure framework, but the inorganic phase was segregated from the organic phase to form a composite hybrid material of ZSM-5 and MCM-41.[26,27] It has also been reported that the compositional change of an inorganic species enhances the hydrothermal stability of the nanostructure frameworks. Yang *et al.* synthesized thermally stable nanoporous metal oxides of TiO_2, ZrO_2, Nb_2O_5, Ta_2O_5, and Al_2O_3 using amphiphilic block copolymer templates.[28,29]

Herein, we report the synthesis of ordered nanoporous

*Corresponding Author. E-mail: ykkwon@inha.ac.kr, kimgj@inha.ac.kr

materials with a hydrothermally stable framework, by exploring the direct conversion of inorganic species by using co-surfactant templating systems. To confer hydrothermal stability on the mesoporous materials, the organic-inorganic hybrids were heat-treated in strongly basic media in an attempt to convert the inorganic species into a protozeolitic material. Since the nanoscopic ordering of the organic-inorganic self-assembly was completely destroyed at high temperature under the strong basic reaction conditions, 1,3,5-trimethylbenzene (TMB) and a nonionic block copolymer of poly(ethylene oxide)-*b*-poly(propylene oxide)-*b*-poly(ethylene oxide) ($EO_{20}PO_{70}EO_{20}$) were added to improve the hydrothermal stability of the organic-inorganic self-assembly during the solid rearrangement process of the inorganic species.

Experimental

Materials. Cetyltrimethylammonium bromide [$C_{16}H_{13}(CH_3)_3$ NBr, CTAB], TMB and $EO_{20}PO_{70}EO_{20}$ triblock copolymer (weight average molecular weight, Mw = 5,800), Ludox HS-40 (colloidal silica, 40 wt% suspension in water), tetrapropylammonium bromide (TPABr), tetrapropylammonium hydroxide (TPAOH) (all from Aldrich), hydrochloric acid, sodium hydroxide, ethanol (all from Sigma) were all used as received. Ludox HS-40 was used as a silica source.

Synthesis of a Mesostructure Prepared with TMB. 6.3 g of TPABr was added to aqueous sodium hydroxide (NaOH) solution (2.5 g NaOH/25 g H_2O) with stirring at 60 °C for 1 hr. TPABr was used as a structure directing template for inducing the protozeolitic order in the framework. Then 10 g of Ludox HS-40 was added and the mixed solution was stirred for an additional 6 hrs at the same temperature. The molar ratio of SiO_2:Na_2O:TPABr:H_2O was 1:0.5:0.35:100. An aqueous solution of CTAB surfactant (7 g CTAB/73 g H_2O) was added to the mixed solution with stirring at the same temperature. The solution was heated to 100 °C and aged at the same temperature for 24 hrs. The pH of the mixed solution was repeatedly adjusted to approximately 10 by the dropwise addition of dilute HCl solution at room temperature. The final mixed solution was heated and aged again at 100 °C for an additional 48 hrs.

The solution was then cooled to room temperature and mixed with TMB (approximately 20 g) and methanol. Then, it was reheated under reflux for an additional 24 hrs. The solution was transferred to a Teflon-coated autoclave in order to bring about the solid rearrangement of the inorganic species in the organic-inorganic self assembly by heat-treating it at 100 °C for 24 hrs, in order to convert it from the inorganic precursor into a protozeolitic material. The solid product was recovered by filtration and dried at 100 °C overnight. The organic phase was removed by calcination at 550 °C for 3 hrs. The final calcined product was conveniently denoted as **1**. Subsequently, the exact same synthetic procedure was repeated without adding TMB and the calcined product obtained by this synthetic method was denoted as **2**.

Synthesis of a Mesostructure Prepared with an Amphiphilic Block Copolymer. The organic phase solution used in the experiment was prepared by dissolving 4.5 g CTAB and $EO_{20}PO_{70}EO_{20}$ in 10 g ethanol with stirring at 50 °C for 1 hr. The molar ratio of CTAB to $EO_{20}PO_{70}EO_{20}$ in the mixtures was varied from 16 to 120. Ludox HS-40 was also used as a silica source. To synthesize the solution of protozeolitic material, 3.15 g of TPABr was dissolved in aqueous NaOH solution (1.25 g NaOH/12.5 g H_2O) with stirring at 50 °C for 1 hr and then 5 g of Ludox HS-40 was added and the solution stirred for an additional 6 hrs at 50 °C. The solution of CTAB and $EO_{20}PO_{70}EO_{20}$ was added to the inorganic precursor solution with stirring. The mixed solution was aged at 100 °C for 3 days. During this aging procedure, the pH of the solution was adjusted to approximately 11 by the dropwise addition of aqueous hydrochloric acid. The final mixture was transferred to a Teflon-coated autoclave and heated to 175 °C for 4 hrs and then washed 3-4 times in liberal amounts of water, decanted, filtered and dried overnight in ambient air. The as-made samples were calcined at 500 °C for 4 hrs in air and the calcined sample with a molar ratio of CTAB/$EO_{20}PO_{70}EO_{20}$ of 56 was denoted as **3**.

Characterization. X-ray analysis was carried out in a Philips PW1847 X-ray diffractometer, operated at 40 kV and 100 mA, using reflection geometry and Cu Kα radiation (wavelength λ = 0.154 nm). The data were measured within the range of scattering angle, 2θ of 1-40°. The as-prepared powders of the specimens were used without further treatment. Transmission electron microscopy (TEM) and scanning electron microscopy (SEM) measurements of the as-received powders of the calcined samples were conducted on a Phillips CM-220 and Hitachi S-4200. The N_2 adsorption and desorption isotherms were determined on a Micrometrics ASAP 2000 sorptometer at -196 °C. The samples were outgassed under a pressure of 10^{-5} torr at 200 °C. The thermal and hydrothermal stabilities of the samples were investigated by exposing them to steam or dry air at high temperatures.

Small angle neutron scattering (SANS) experiments were carried out on the facility at the HANARO center in KAERI in Korea with a two dimensional position sensitive 65 × 65 cm^2 detector. The equipment in question employs a circular pinhole collimation with a Bi/Be filter. The neutron scattering intensity was measured using a neutron wavelength of 5.08 Å with a wavelength resolution $\Delta\lambda/\lambda$~1.8% at a sample-to-detector distance of 3 m, covering a Q ($4\pi \sin\theta/\lambda$ where 2θ is scattering angle) range of 0.01-0.24 $Å^{-1}$. A quartz cell with a path length of 2 mm was used as the sample container, and the samples were loaded at room temperature. The scattered intensities were converted to an absolute dif-

ferential scattering cross section per unit sample volume after calibration with a silica standard (NIST). The data were multiplied by a factor of ~10^1 to $10^{1.5}$ to avoid overlapping between them. The backgrounds from D_2O and the quartz cell were also subtracted.

Results and Discussion

Nanostructures Prepared with TMB. Figure 1(a) and (b) illustrate the typical XRD scans of **1** and **2**, respectively. Figure 1(a) consists of a series of small angle Bragg peaks up to a 2θ value of nearly 7°. These peak intensities appeared to be due to the long-range nanoscopic order of the pore structure and were indexed by a two-dimensional hexagonal lattice with parameters of $a = b = 40.5$ Å. These data indicate that the mesopores of **1** are nicely arranged in a two dimensional hexagonal lattice. The weak peaks at 2θ values of nearly 7.5°, 10°, and 23° may be due to the presence of the small amount of ZSM-5 crystals which existed along with mesoporous **1**. The presence of the long-range order of the pore structure of **1** also revealed that the nanoscopic ordering of the organic-inorganic self-assembly persisted during the heat treatment of the inorganic species at 175 °C under the basic reaction conditions.

Figure 1(b) shows a series of sharp Bragg peaks at 2θ= 8.1, 9.0, and 23.4° which correspond to the 011, 200, and 033 peaks of the ZSM-5 zeolite crystal structure, respectively. The absence of the small angle X-ray scattering peaks indicated that the nanoscopic ordering of the pore structure of the calcined sample **2** was absent. The wide angle X-ray diffraction (XRD) data of the specimens prepared without the addition of TMB were also measured before and just after the heat treatment of the inorganic species at 175 °C. The XRD data measured from the specimen obtained before the heat treatment were quite similar to those observed in Figure 1(a), showing a series of sharp Bragg peaks in the small angle region, whereas no small angle X-ray peaks were found in the specimen obtained just after the heat treatment. These results revealed that the organic-inorganic self-assembly was collapsed during the heat treatment of the inorganic species at 175 °C in the basic reaction media.

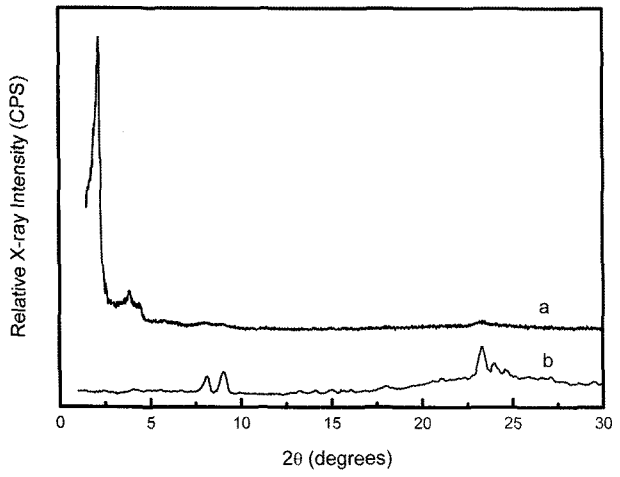

Figure 1. The measured XRD data of (a) **1** and (b) **2**.

Table 1. Physicochemical Properties of the Mesoporous Materials. Pore Volume, Pore Size Distribution and BET Surface Area were Determined by the N_2 Adsorption-Desorption Measurements

Samples	$d(100)^b$ (Å)	BET Surface Area (m^2/g)	Pore Diameter[c] (Å)	Pore Volume (cm^3/g)	Wall Thickness[d] (Å)
1	39.8	920	33.0	1.0	13.0
1[e]	41.1	890	34.9	0.9	12.6
2	39.3	982	29.5	1.0	15.9
3	45.1	957	36.9	0.9	15.2

*Prepared without the solid rearrangement in an autoclave at 175 °C. [b]Calculated from the XRD data, [c]Determined by the BET measurements. [d]a_0 - pore diameter where a_0 was defined as $2d(100)/3^{1/2}$. [e]Steamed at 800 °C for 3 hrs.

During the heat treatment in the autoclave, we could not adjust the pH of the solution of the organic-inorganic self-assembly, which continuously increased with increasing reaction time, due to the additional NaOH, produced by the hydrolysis and thermal condensation reaction of the inorganic species. At high pH or in strongly basic reaction media, the inorganic species, which was associated with the organic phase by electrostatic force, was dissolved, and the long-range nanoscopic order of the organic-inorganic self-assembly no longer persisted in the solution. The dissolved inorganic species was segregated and crystallized to form ZSM-5 crystals during the thermal treatment in the autoclave. On the other hand, the segregated organic phase was completely removed during the process of calcination at 550 °C.

In the case of **1**, the absence of the XRD peaks reveals the amorphous nature of the silica framework phase. Although the organic-inorganic self-assembly was heat-treated in the autoclave at 175 °C in basic reaction media, in an attempt to induce the molecular reorganization of the inorganic species, the inorganic species could not be crystallized in the limited spaces within the organic-inorganic hybrids. The broadness of the amorphous scattering peaks, centered at $2\theta \approx 23°$, indicates the short range, local order of the protozeolitic inorganic phase in the framework of **1**. This short range, local order of the protozeolitic inorganic phase is believed to be similar, in structure, to that of the zeolite seed materials, recently reported by Pinnavaia *et al.*.[21,22]

Nanostructures Prepared with $EO_{20}PO_{70}EO_{20}$. Figure 2 shows the SANS intensity profiles of the D_2O solutions of the mixed surfactants of $EO_{20}PO_{70}EO_{20}$ and CTAB at various molar ratios of CTAB to $EO_{20}PO_{70}EO_{20}$. In Figure 2(a), the

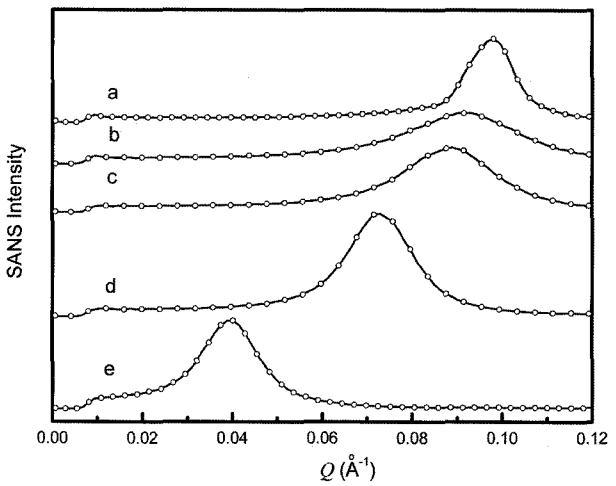

Figure 2. Typical SANS data of the D_2O solutions of the mixed surfactants of $EO_{20}PO_{70}EO_{20}$ and CTAB at various molar ratios of CTAB/$EO_{20}PO_{70}EO_{20}$ of (a) 100/0, (b) 72/1, (c) 56/1, (d) 16/1, and (e) 0/100.

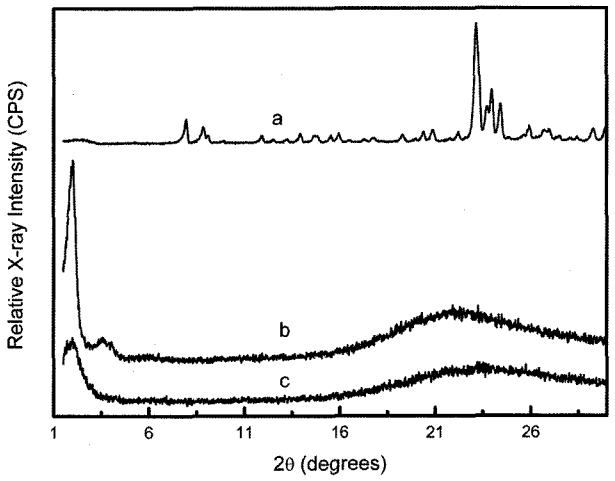

Figure 3. The measured XRD scans of the calcined nanoporous materials, prepared based on the mixed micellar solutions organic templates at a molar ratio of CTAB to $EO_{20}PO_{70}EO_{20}$ of (a) 16, (b) 56 **(3)**, and (c) 72.

solution of the CTAB surfactant with a concentration of 30 wt% gave an intense peak at Q ($= 4\pi \sin\theta/\lambda$ where 2θ is the scattering angle)$\approx$0.098 Å^{-1} which corresponded to an intermicellar spacing of 64.1 Å. $EO_{20}PO_{70}EO_{20}$ was added to the CTAB solution, so as to form the mixed micellar solutions of CTAB and $EO_{20}PO_{70}EO_{20}$ with a concentration of 30 wt%. When the amount of $EO_{20}PO_{70}EO_{20}$ in the mixed solutions was increased by a molar ratio of CTAB/$EO_{20}PO_{70}EO_{20}$ of 16, the position of the SANS peak was lowered to $Q\approx$0.073 Å^{-1}. Note that the solution of $EO_{20}PO_{70}EO_{20}$ with a concentration of 30 wt% gave a SANS peak at Q ($= 4\pi \sin\theta/\lambda$ where 2θ is the scattering angle)$\approx$0.040 Å^{-1} which corresponded to an intermicellar spacing of 157.1 Å. The continuous decrease in the position of the SANS peak as the amount of $EO_{20}PO_{70}EO_{20}$ in the mixed surfactant solution was increased confirmed that $EO_{20}PO_{70}EO_{20}$ molecules were successfully incorporated to form mixed micelles with the CTAB surfactant.

Figure 3 illustrates the typical XRD scans of the calcined nanoporous materials prepared based on the mixed micellar organic templates at a molar ratio of CTAB to $EO_{20}PO_{70}EO_{20}$ of (a) 16; (b) 56 (**3**) and (c) 72. Curve a of Figure 1 shows a series of sharp Bragg peaks at $2\theta \approx$ 8, 9, and 23° similar to those shown in Figure 1(b), which appeared to be due to a ZSM-5 zeolite crystal structure. The absence of the series of small angle Bragg peaks also indicated that the nanoscopic ordering of the pore structure of their calcined samples had completely collapsed. This might have been caused by the disordered internal arrangement of the mixed micelles with excess $EO_{20}PO_{70}EO_{20}$. In Figure 3(b), we found an intense Bragg peak near $2\theta = 2°$ and weak higher order peaks up to approximately 7°. These peaks determined the unit cell parameters of the hexagonal lattice to be $a = b = 44.2$ Å. The presence of these SAXS peaks also indicates that the nanoscopic ordering of the organic-inorganic self-assembly of **3** persists during the heat treatment of the inorganic species under the basic reaction conditions. The broadness and weakness of the SAXS peak found in Figure 3(c) appeared to be due to the disordered morphology of the pore structure of the calcined nanostructure prepared at a molar ratio of CTAB to $EO_{20}PO_{70}EO_{20}$ of 72. The existence of an amorphous halo in the wide angle region indicates that the organic phase was not dissolved and segregated from the inorganic species, but that nanoscopic ordering of the pore structure was not highly developed, because of the lack of $EO_{20}PO_{70}EO_{20}$ in the mixed micelles, which reduced the hydrothermal stability of the organic-inorganic self-assembly during the heat treatment.

We speculated that the electrostatic molecular interactions between $EO_{20}PO_{70}EO_{20}$ and CTAB enhanced the molecular packing density by the addition of $EO_{20}PO_{70}EO_{20}$ to the CTAB micellar solutions, especially in the hydrophobic core, leading to a hard-gel type micellar formation. With its tightly-coiled molecular conformation, the organic-inorganic template may not be ruptured even during the solid phase conversion of the inorganic precursors into the protozeolitic species. The successful incorporation of the non-ionic $EO_{20}PO_{70}EO_{20}$ into the cationic CTAB solution depends on the molar ratio of the two components with their respective molecular weights. The degree of incorporation changes the molecular packing density or interfacial curvature of the mixed micelles which, in turn, has a significant effect on the persistence of the nanoscopic ordering of the organic-inorganic templates during the heat treatment in the autoclave.

Hydrothermal Stability. To check the thermal stability of **1** and **3**, they were exposed to dry air at high temperatures. The typical XRD data for **1** after being exposed to dry

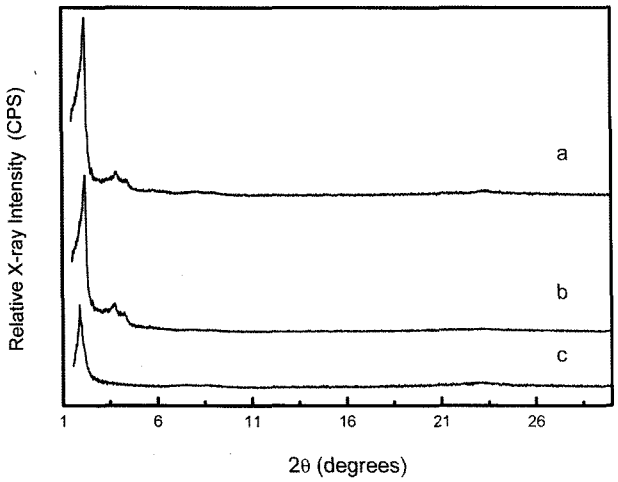

Figure 4. Typical XRD data of **1**: (a) after being exposed to dry air at 900 °C for 5 hrs, (b) after being placed in boiling water for 24 hrs, and (c) after being placed in 0.5 N-NaOH solution for 5 hrs.

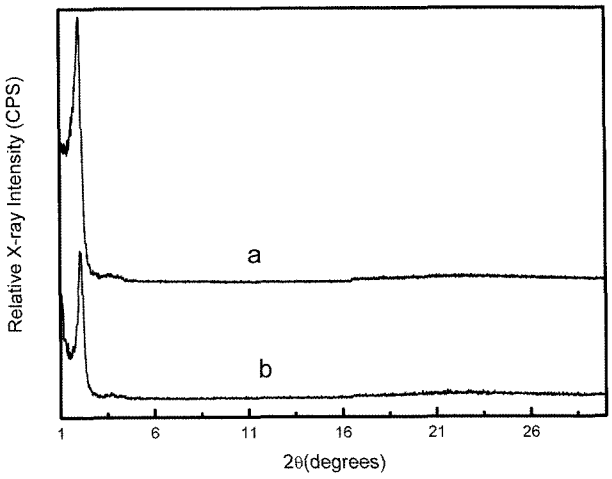

Figure 5. Typical XRD data of **3**: (a) after being placed in boiling water for 24 hrs and (b) after being placed in 0.5 N-NaOH solution for 4 hrs.

air at 900 °C for 5 hrs are shown in Figure 4(a). These data are almost the same as those seen in Figure 1(a), confirming the thermal stability of **1**. Figure 4(b) and (c) also show the XRD data of **1**, following its treatment in boiling water for 24 hrs and 0.5 N-NaOH solution for 5 hrs, respectively. **1** was also placed in steam at 800 °C for 5 hrs and its XRD pattern following this treatment was almost the same as that seen in Figure 4(b), confirming the steam stability of **1**. The intensities and positions of the 100 peaks in Figure 4(b) and (c) were almost the same as those obtained from the untreated **1**, indicating the hydrothermal stability of **1** in boiling water or 0.5 N-NaOH solution. The small shift of the 100 peak and small decrease in its intensity in Figure 4(c) were probably due to the partial dissolution of the pore structure which enlarged the distance between the pores. Compared to **1**, MCM-41 and SBA-15 with their thick framework walls, were completely dissolved in 0.5 N-NaOH solution.

Figure 5 shows the XRD data of **3**; (a) after being treated in boiling water for 24 hrs; and (b) after being treated in 0.5 N-NaOH solution for 4 hrs. The XRD data in Figure 5(a) and (b) are almost the same as those observed in Figure 3(a), indicating the hydrothermal stability of the **3** both in boiling water and in alkali solution. In these data, the diffracted intensity of the peak at $2\theta \approx 2°$ for **3**, which is shown in Figure 3(a), was slightly reduced in Figure 5(a) and (b), again due to the partial dissolution of the pore structure. These reductions were similar to those shown in Figure 4(b) and (c). The peak shift toward the small angle region also indicates the enlarged distance between the pores.

It is been well known that MCM-41 contains agglomerates of round particles in its SEM morphology. Figure 6(a) and (b) show the SEM images of **1** and **3**, showing the presence of agglomerates of round particles which are almost the same as those seen in the case of MCM-41, confirming the

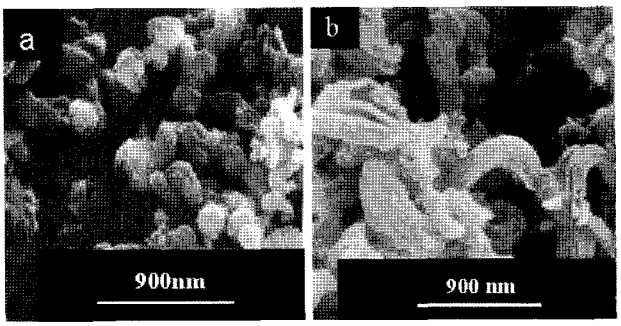

Figure 6. SEM images of **1** and **3**.

mesoscopic ordering of these materials. In addition, the crystal morphology of the ZSM-5 crystal structure was absent in this image, indicating that the inorganic species remains amorphous after the heat treatment at 175 °C under the basic reaction conditions. The SEM data were coincident with those measured from the XRD data, shown in Figure 1(a) and (c).

Figure 7(a) and (b) show the typical TEM micrographs of **1** and **3**. The images show a nicely arranged uniform hexagonal array of pores on the nanometer scale. Together with the nicely ordered hexagonal nanoporous structure, we also observed partially disordered or slightly collapsed areas, which appeared to be due to the heat treatment under the basic reaction conditions. The coexistence of a disordered porous structure reduces the structural perfection of the pore structure, which may be related to the broadness and weakness of the small angle Bragg peaks in Figure 1. The electron diffraction (ED) pattern of the **1**, recorded along the 001 zone axis, shown in the inset of Figure 6(a), reveals only a diffuse amorphous halo, indicating that the framework of **1** was comprised of the amorphous protozeolitic nuclei. This ED pattern is coincident with the data obtained in the XRD

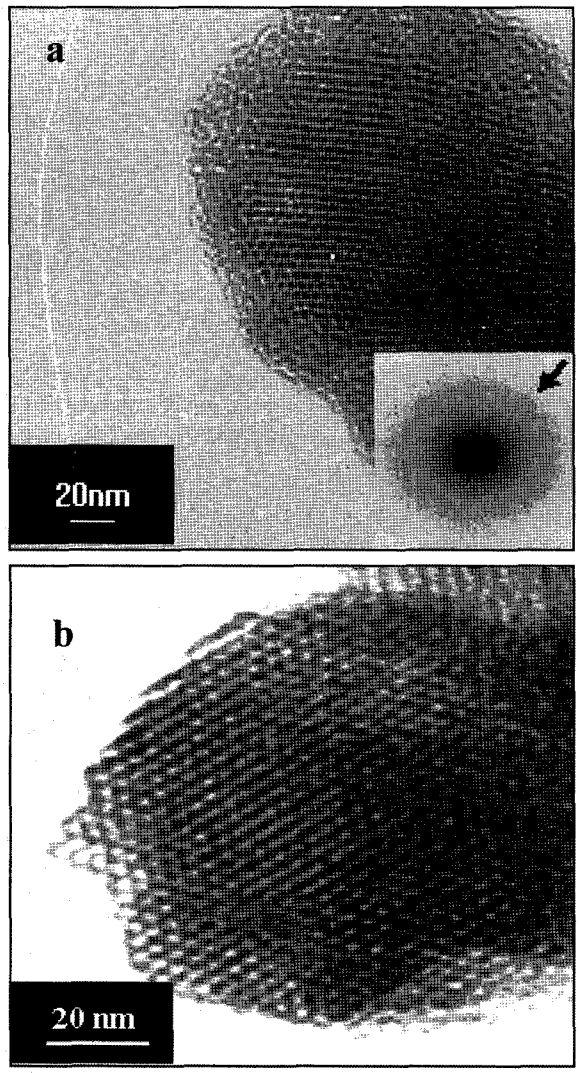

Figure 7. TEM micrographs of **1** and **3**.

measurements.

Figure 8(a) and (b) show the N_2 adsorption-desorption isotherms of **1** and **3**. The data show a type IV adsorption isotherm behavior with H1 hysteresis. The initial steep increase in the relative value of P/P_0 may be due to the existence of the zeolitic nuclei within the framework. **1** and **3** had N_2 BET surface areas of 920 and 956 m^2/g, respectively, which were slightly smaller than that of MCM-41. The reduction in the BET surface areas of **1** and **3** may be due to the distortion of the pore structure, which occurred during the solid rearrangement process in the frameworks. Based on the $d(100)$ spacing calculated from the XRD measurements and the mean pore size determined by N_2 adsorption, the thicknesses of the framework walls of **1** and **3** were estimated to be approximately 12 and 14 Å, respectively, which were similar to that of MCM-41.

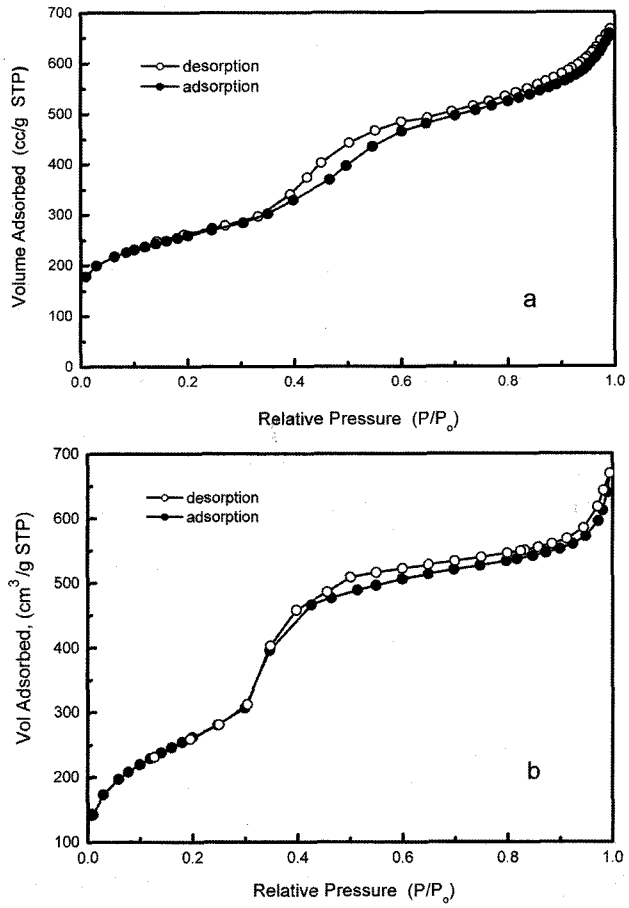

Figure 8. N_2 adsorption-desorption isotherms of **1** and **3**.

Conclusions

Using the synthetic method proposed in the study, we successfully demonstrated that the hydrothermal stability of the mesoporous materials was derived from the heat treatment of the inorganic species of the organic-inorganic self-assembly under the basic reaction conditions. The persistence of the long-range ordering of the organic-inorganic self-assembly was obtained by the addition of TMB or $EO_{20}PO_{70}EO_{20}$ which enhanced the hydrothermal stability of the organic-inorganic self-assembly during its treatment in the autoclave at 175 °C and pH ≈ 11 or 12. The molar ratio between $EO_{20}PO_{70}EO_{20}$ and CTAB determines the morphology of the calcined pore structures. Our preliminary data showed that the catalytic activity of these mesoporous materials was excellent for both large and small molecules and that they can be used as a catalyst in various applications. Their catalytic activity will be described in a separate publication.

Acknowledgements. This work was supported by Korea Research Foundation Grant (KRF-2004-003-D00095).

References

(1) D. W. Breck, *Zeolite Molecular Sieves,* Wiley, New York, 1974.
(2) R. M. Barrer, *Hydrothermal Chemistry of Zeolites*, Academic Press, London, 1982.
(3) S. T. Wilson, B. M. Lok, C. A. Messina, T. K. Cannan, and E. M. Flanigen, *J. Am. Chem. Soc.,* **104**, 1146 (1982).
(4) H. Gies and B. Marler, *Zeolites,* **12**, 42 (1992).
(5) C. T. Kresge, M. E. Leonowicz, W. J. Roth, J. C. Vartuli, and J. S. Beck, *Nature*, **352**, 710 (1992).
(6) J. S. Beck, J. C. Vartuli, W. J. Roth, M. E. Leonowicz, C. T. Kresge, K. D. Schmitt, C. T-W. Chu, D. H. Olson, E. W. Sheppard, S. B. McCullen, J. B. Higgins, and J. L. Schlenker, *J. Am. Chem. Soc.,* **114**, 10834 (1992).
(7) Q. Huo, R. Leon, P. M. Petroff, and G. D. Stucky, *Science,* **268**, 1324 (1995).
(8) Q. Huo, D. I. Margolese, and G. D. Stucky, *Chem. Mater.*, **8**, 1147 (1996).
(9) S. Schacht, Q. Huo, I. G. Voight-Martin, G. D. Stucky, and F. Schuth, *Science,* **273**, 768 (1996).
(10) J. Aguado, D. P. Serrano, M. D. Romero, and J. M. Escola, *Chem. Commun.,* 725 (1996).
(11) A. Corma, M. S. Grande, V. Gonzalez-Alfaro, and A. V. Orchilles, *J. Catal.,* **159**, 375 (1996).
(12) M. S. Whang, Y. K. Kwon, and G.-J. Kim, *J. Ind. Eng. Chem.,* **8**, 262 (2002).
(13) S. A. Bagshaw, E. Prouzet, and T. J. Pinnavaia, *Science,* **269**, 1242 (1995).
(14) S. A. Bagshaw and T. J. Pinnavaia, *Angew. Chem. Int. Ed. Engl.,* **35**, 1102 (1996).
(15) D. Zhao, Q. Huo, J. Feng, B. F. Chmelka, and G. D. Stucky, *J. Am. Chem. Soc.,* **120**, 6024 (1998).
(16) D. Zhao, J. Feng, Q. Huo, N. Melosh, G. H. Fredrickson, B. F. Chmelka, and G. D. Stucky, *Science,* **279**, 548 (1998).
(17) G. S. Attard, J. C. Glyde, and C. G. Göltner, *Nature,* **378**, 377 (1995).
(18) M. Antonietti and C. G. Göltner, *Angew. Chem. Int. Ed. Engl.,* **36**, 516 (1997).
(19) K. R. Kloesstra, H. W. Zandbergen, J. C. Jansen, and H. van Bekkum, *Microporous Mater.,* **6**, 287 (1996).
(20) K. R. Kloesstra, H. van Bekkum, and J. C. Jansen, *Chem. Commum.,* 2281 (1997).
(21) Y. Liu, W. Zhang, and T. J. Pinnavaia, *J. Am. Chem. Soc.,* **122**, 8791 (2000).
(22) Y. Liu, W. Zang, and T. J. Pinnavaia, *Angew. Chem. Int. Ed. Engl.,* **40**, 1255 (2001).
(23) Z. Zhang, Y. L. Zhu, R. Wang, Y. Yu, S. Qiu, D. Zhao, and F.-S. Xiao, *Angew. Chem. Int. Ed. Engl.,* **40**, 1258 (2001).
(24) L. Huang, W. Guo, P. Deng, Z. Xue, and Q. Li, *J. Phys. Chem.,* **104**, 2817 (2000).
(25) R. Ryoo, J. M. Kim, and C. H. Shin, *J. Phys. Chem.,* **100**, 17718 (1996).
(26) A. Karlsson, M. Stöcker, and R. Schmidt, *Micropor. Mesopor. Mater.,* **27**, 181 (1999).
(27) A. Karlsson, M. Stöcker, and K. Schäfer, *Stud. Surf. Sci. Catal.,* **125**, 61 (1999).
(28) P. Yang, D. Zhao, D. I. Margolese, B. F. Chmelka, and G. D. Stucky, *Nature,* **396**, 152 (1998).
(29) P. Yang, D. Zhao, D. I. Margolese, B. F. Chmelka, and G. D. Stucky, *Chem Mater.,* **11**, 2813 (1999).